






Article

Beyond the Scavenging of Reactive Oxygen Species (ROS): Direct Effect of Cerium Oxide Nanoparticles in Reducing Fatty Acids Content in an In Vitro Model of Hepatocellular Steatosis

Marina Parra-Robert ^{1,†}, Eudald Casals ^{2,†} , Nuria Massana ¹ , Muling Zeng ², Meritxell Perramón ¹ , Guillermo Fernández-Varo ^{1,3}, Manuel Morales-Ruiz ^{1,3,4}, Víctor Puntès ^{5,6,7}, Wladimiro Jiménez ^{1,3}  and Gregori Casals ^{1,4,*} 

¹ Service of Biochemistry and Molecular Genetics, Hospital Clinic Universitari, Centro de Investigación Biomédica en Red de Enfermedades Hepáticas y Digestivas (CIBERehd), Institut d'Investigacions Biomèdiques August Pi i Sunyer (IDIBAPS), 08905 Barcelona, Spain

² School of Biotechnology and Health Sciences, Wuyi University, Jiangmen 529020, China

³ Departament of Biomedicine, University of Barcelona, 08905 Barcelona, Spain

⁴ Working group for the biochemical assessment of hepatic disease-SEQC^{ML}, 08036 Barcelona, Spain

⁵ Vall d'Hebron Research Institute (VHIR), 08035 Barcelona, Spain

⁶ Institut Català de Nanociència i Nanotecnologia (ICN2), CSIC, The Barcelona Institute of Science and Technology (BIST), Campus UAB, Bellaterra, 08193 Barcelona, Spain

⁷ Institució Catalana de Recerca i Estudis Avançats (ICREA), 08010 Barcelona, Spain

* Correspondence: casals@clinic.cat; Tel.: +34-932275400-2667

† These authors contributed equally to this work.

Received: 13 July 2019; Accepted: 27 August 2019; Published: 29 August 2019



Abstract: Nonalcoholic fatty liver disease (NAFLD) is characterized by hepatic accumulation of lipids. Antisteatotic effects of cerium oxide nanoparticles (CeO₂NPs) have recently been shown in animal models of liver disease. However, it is unclear whether the activity of CeO₂NPs is related solely to the decrease in oxidative stress or, in addition, they directly decrease liver fatty acid accumulation. To address this question, in this work, we used an in vitro model of hepatocellular steatosis, exposing HepG2 cells to oleic and palmitic acid. Cell uptake of CeO₂NPs and their effect on oxidative stress and viability of hepatic cells cultured with H₂O₂ were also evaluated. Results show that CeO₂NPs were uptaken by HepG2 cells and reduced oxidative stress and improved cell viability. Treatment with oleic and palmitic acid increased lipogenesis and the content of different fatty acids. CeO₂NPs reduced palmitic and stearic acid and most fatty acids consisting of more than 18 carbon atoms. These effects were associated with significant changes in elongase and desaturase activity. In conclusion, CeO₂NPs directly protected HepG2 cells from cell injury in oxidative stress conditions and reduced fatty acid content in steatotic conditions by inducing specific changes in fatty acid metabolism, thus showing potential in the treatment of NAFLD.

Keywords: nonalcoholic fatty liver disease; steatosis; liver; cerium oxide nanoparticles; oxidative stress

1. Introduction

Nonalcoholic fatty liver disease (NAFLD) is characterized by hepatic lipid accumulation (steatosis), mainly in the form of triglycerides, and covers a wide spectrum of liver disease that ranges from simple hepatic steatosis (nonalcoholic fatty liver, NAFL) to nonalcoholic steatohepatitis (NASH), the last being

characterized by the appearance of inflammation and a higher risk of progression to more advanced forms including fibrosis, cirrhosis and hepatocellular carcinoma (HCC) [1].

Oxidative stress plays a role in the molecular mechanisms behind the progression of NAFLD. In this regard, the pathogenesis of NAFLD may be explained by a multiple-hit hypothesis [2]. In the context of excess energy, fatty acids (FAs) are esterified into triacylglycerides and stored in lipid droplets in the liver. The multiple-hit hypothesis considers multiple insults, including insulin resistance, adipokines, nutritional factors or gut microbiota that act together on genetically predisposed subjects in the development and progression of the disease [2,3]. These insults are associated with increased oxidative stress, proinflammatory cytokines and adipocytokines, leading to hepatocyte injury, inflammation and fibrosis [4,5]. The hepatic accumulation of free FA, lipid peroxidation products (reactive aldehydes and oxysterols) and reactive oxygen species (ROS) contribute to the development and progression of NAFLD from simple steatosis to NASH by impairing mitochondrial function, energy balance and biogenesis adaptation to chronic injury [6,7].

The current treatment of NAFLD consists of diet and lifestyle interventions, such as healthy eating habits and physical activity, to achieve weight loss and the control of its associated cardio-metabolic risk factors [8–10]. However, reinforcement of these interventions by pharmacological therapies would be useful in the management of patients. Unfortunately, effective treatment options for NAFLD remain limited [1]. At present, there are no pharmacological treatments licensed for the reduction of liver steatosis, and the American and European guidelines for the management of NAFLD patients are only supportive of the use of two drugs: pioglitazone in patients with NASH with or without *diabetes mellitus*, and vitamin E, a recognized antioxidant, in nondiabetic patients with NASH [9,10]. The identification of strategies directed to halt NAFLD progression are, therefore, an urgent need.

In recent years, the antioxidant properties of cerium oxide nanoparticles (CeO_2NPs) have been widely described in the literature [11–16]. CeO_2NPs , which display minimal toxicity to normal tissues and provide cellular protection from various forms of ROS and irradiation [17], have emerged as a powerful antioxidant therapeutic tool in the prevention and treatment of oxidative-stress-related diseases. The interest in CeO_2NPs include their natural advantages over other antioxidants since CeO_2NPs participate catalytically in redox cycles, which mean that they are not consumed during reaction, and thus, they can be used at low doses. Their oxygen storage capacity has proven useful in scavenging free radicals as soon as they are generated in situations of metabolic imbalance [12]. In this context, it has been shown that CeO_2NPs exhibit superoxide dismutase [18], catalase [19] and peroxidase [20] mimetic activities. Thus, CeO_2NPs have been postulated as a possible treatment for pathologies associated with chronic oxidative stress and inflammation such as cancer, cardiac disease and neurodegenerative disease, among others [21–25]. Interestingly, after their administration, CeO_2NPs are accumulated mainly in the liver and for long periods of time [26,27]. Recent studies carried out in our laboratory show that CeO_2NPs decrease portal hypertension, liver inflammatory response and hepatic steatosis in a rat model of liver fibrosis induced by CCl_4 [27]. Additionally, oral administration of CeO_2NPs to a NAFLD rat model associated with neonatal monosodium-glutamate-induced obesity has been reported to decrease body weight and liver steatosis [28]. However, it is unknown whether this antisteatotic effect is due to a direct effect of CeO_2NPs in the liver. In the current study, we used an in vitro model system of cultured human hepatic cells (HepG2) to test the hypothesis of whether CeO_2NPs can directly reduce FA accumulation in the absence of other stimuli.

2. Materials and Methods

2.1. Synthesis and Characterization of CeO_2NPs

2.1.1. Synthesis

CeO_2NPs of 4 nm of mean diameter were synthesized in aqueous media by the chemical precipitation of Cerium (III) Nitrate Hexahydrate ($\text{Ce}(\text{NO}_3)_3$) under basic conditions. Briefly, 10 mM of Cerium (III) Nitrate Hexahydrate was dissolved in 97 mL of Milli-Q H_2O at room temperature.

The solution was left under stirring for about 30 min. To this, 3 mL of tetramethylammonium hydroxide (TMAOH) (1.0 ± 0.02 M in H_2O) was added under stirring (final TMAOH concentration of 30 mM), and the mixture was left under stirring overnight. Afterward, nanoparticles (NPs) were purified by centrifugation (20,000 g, 10 min) and resuspended in an aqueous solution of 1 mM TMAOH. In this synthesis, the conversion of initial cerium precursor to CeO_2 NPs is nearly complete, as determined by UV-VIS spectroscopy and inductively coupled plasma mass spectrometry (ICP-MS).

2.1.2. Albumin Conjugation

Electrostatically stabilized CeO_2 NPs have a strong tendency to aggregate at physiological pH, which can result in deleterious immune responses [29]. To avoid this, Human Serum Albumin (HSA) was conjugated to the CeO_2 NPs surface prior to their use. Albumin was added at 100-fold the amount needed to cover the surface of CeO_2 NPs to ensure complete albumin corona formation.

2.1.3. Characterization

The NPs' size was determined using high-resolution transmission electron microscopy (HR-TEM) with a microscope JEOL JEM 2010F at 200 kV (Tokyo, Japan), and further image analysis using the Image J free software (National Institutes of Health, Bethesda, MD, USA). The surface charge of the NPs was characterized in a Z-sizer (Malvern, Worcestershire, UK). The crystal structure was analyzed by X-ray powder diffraction (XRD) (Xpert Pannalytical, MA, USA), and the light interaction by UV-VIS spectroscopy (Shimadzu, Kyoto, Japan).

2.2. Cell Culture

HepG2 cells were obtained from American Type Culture Collection (ATCC, Manassas, VA, USA). This immortalized human hepatocellular stable cell line can be repeatedly frozen, thawed and propagated. HepG2 cells were seeded into either 96-well culture plates for cell bioavailability analysis, 24-well culture plates for ROS measurements, six-well culture plates for steatosis induction and nanoparticles cell uptake evaluation or 75 cm^2 flasks for measurements of oxysterols. After seeding, cells were grown to confluence in Dulbecco's Modified Eagle Medium (DMEM), supplemented with 10% fetal bovine serum (FBS), 50 U/mL penicillin and 50 μ g/mL streptomycin, in a humidified atmosphere of 5% CO_2 at 37 °C. Thereafter, the cells were switched to serum-free DMEM for 16 h. For cell stimulation and treatment, old medium was removed and replaced with medium, medium containing 1.5 mM H_2O_2 (Sigma-Aldrich, St. Louis, MO, USA) or medium containing 1.5 mM H_2O_2 and CeO_2 NPs. Cells were incubated for the indicated time points and then harvested for biochemical or molecular assays. All experiments were repeated at least three times.

2.3. Internalization of CeO_2 NPs in HepG2 Cells

The uptake of CeO_2 NPs by the cell cultures was assessed using bright-field and dark-field TEM images. HepG2 cells were seeded (1.5×10^6 cells/well) in six-well plates and incubated with or without CeO_2 NPs (10 μ g/mL) for 24 h. Thereafter, cells were fixed in a 0.1 M phosphate buffer containing 2.5% glutaraldehyde and 2% paraformaldehyde. Cells were embedded in Spur's resin and thin sections (50–55 nm) were cut and placed on copper grids and then stained with uranyl acetate and lead citrate. After staining, the sections were examined using a low-electron-power microscope to increase contrast in a JEOL-1010 TEM (JEOL, Tokyo, Japan) operated at 80 kV and equipped with a BioScan camera (Gatan, CA, USA).

2.4. Cell Viability Analysis

Cell viability was assessed using the MTS (3-(4,5-dimethylthiazol-2-yl)-5-(3-carboxymethoxyphenyl)-2-(4-sulfophenyl)-2H-tetrazolium) technique (CellTiter 96; Promega, Madison, WI, USA) according to the manufacturer's instructions. In brief, cells were seeded

(1×10^5 cells/well) in 96-well plates and, after overnight starvation, cells were treated with medium, H_2O_2 (1.5 mM) or H_2O_2 and CeO_2 NPs (10 μ g/mL) for 90 min at 37 °C. Then, cells were washed twice with Hank's Balanced Salt Solution (HBSS) and CellTiter reagent was added to each well. After incubation for 3 h at 37 °C to allow cells to bioreduce MTS into formazan, the absorbance of formazan, measured at 490 nm (SpectraMax 340, Molecular Devices, Sunnyvale, CA), is directly proportional to the number of living cells in culture.

2.5. Reactive Oxygen Species Measurement

Fluorescence spectrophotometry was used to measure ROS, with 2',7'-DCF-DA (2',7'-dichlorofluorescein diacetate) as the probe (Sigma-Aldrich, St. Louis, MO, USA). DCF-DA readily diffuses through the membrane and is enzymatically hydrolyzed by intracellular esterases to the nonfluorescent DCFH (2',7'-dichlorodihydrofluorescein), which can then be rapidly oxidized to fluorescent DCF in the presence of ROS. HepG2 cells were seeded in 24-well plates and, after overnight starvation, cells were incubated alone or with H_2O_2 (1.5 mM) in the presence of CeO_2 NPs (1 μ g/mL) or medium for 90 min. Thereafter, cells were washed with HBSS and incubated with 10- μ M DCF-DA in Hanks Balanced Salt Solution for 40 min at 37 °C in the dark. The supernatant was collected to measure the production of ROS, and the intensity of DCF fluorescence was immediately read in a fluorescence spectrophotometer (FLUOstar OPTIMA; BMG LABTECH, Ortenberg, Germany) at 485 nm for excitation and at 520 nm for emission.

2.6. Oxysterols Measurements

Cells were seeded in 75-cm² flasks and, after overnight starvation, incubated with medium, H_2O_2 (1.5 mM) or H_2O_2 and CeO_2 NPs (1.5 mM; 10 μ g/mL) for 90 min. Afterward, cell pellets were obtained by trypsinization and the oxysterol content was analyzed. Cholesterol, cholesterol d7, 7 β -hydroxycholesterol, 7-ketocholesterol, 25-hydroxycholesterol and 5 α -cholestane were purchased from Steraloids (Newport, RI). Lipids were extracted from HepG2 cells with chloroform–methanol (2:1 vol/vol) in the presence of butylated hydroxytoluene (0.005%) as an antioxidant. 5 α -cholestane and cholesterol-d7 were added as internal standards. After centrifugation, the lower phase was evaporated under a nitrogen stream and extracts were silylated with N,O-bis-(trimethylsilyl)-trifluoroacetamide containing 1% trimethylchlorosilane (Sigma). Gas chromatography mass spectrometry (GC–MS) analyses were performed on a Shimadzu GCMS QP2010 Ultra instrument (Kyoto, Japan). Sterols were separated in a Sapines-5MS+ capillary column (30 m \times 0.25 mm internal diameter \times 0.25 μ m film thickness) from Teknokroma with helium as a carrier gas at a constant velocity of 50 cm/s. The temperature program was programmed to begin at 50 °C and this temperature was maintained for 3 min. Then, it was elevated at a rate of 80 °C min⁻¹ to 240 °C, before being increased at 2 °C min⁻¹ to a temperature of 290 °C and finally, maintained for 2 min at 290 °C. The ion source and transfer line temperatures were set to 270 °C and 280 °C, respectively. Mass detector was operated in selected ion monitoring (SIM) mode and identification of the analytes was achieved by GC retention time comparison with reference standards. No oxidation of d7-cholesterol to deuterated oxysterols was observed during the analytical procedure.

2.7. Induction of Steatosis in HepG2 Cells with Oleic and Palmitic Acids

HepG2 cells were seeded (1.5×10^6 cells/well) in six-well plates and grown to confluence as described above. After overnight starvation, the medium was changed to 10% FBS medium or 10% FBS medium with 1.33 mM oleic acid (OA) and 0.67 mM palmitic acid (PA) with or without CeO_2 NPs (10 μ g/mL) for 24 h to induce the hepatosteatotic condition [30,31]. Three cell cultures were compared: (i) cells incubated with 10% FBS medium, (ii) cells incubated with 10% FBS medium and OA+PA, (iii) cells incubated with 10% FBS and OA+PA and CeO_2 NPs (10 μ g/mL).

2.8. Total FA Measurements

Lipids were extracted from HepG2 cells with chloroform–methanol (2:1 vol/vol) in the presence of butylated hydroxytoluene (0.005%). C19:0 (Sigma Aldrich, Madrid, Spain) was used as an internal standard. After homogenization, samples were placed on an orbital shaker for 20 min at room temperature and centrifuged for 10 min at 10,000 rpm. The supernatant was mixed with 250 μ L of water, vortexed and centrifuged again for 10 min at 10,000 rpm. The lower organic phase was retrieved, evaporated under a nitrogen stream and redissolved in a mixture of methanol:hexane (4:1, v/v). Acetyl chloride was added and FA methyl ester (FAME) obtained by heating the samples at 100 °C for 1 h. GC–MS analyses were performed on a Shimadzu GCMS QP2010 Ultra instrument (Kyoto, Japan). Final extracts were injected into the gas chromatograph interfaced with a mass selective detector. Chromatographic separation was achieved on a Sapines-5MS+ capillary column (30 m \times 0.25-mm internal diameter \times 0.25- μ m film thickness) from Teknokroma (Barcelona, Spain) with helium as a carrier gas at a constant velocity of 50 cm/s. The temperature program was set to begin at 50 °C and this temperature was maintained for 3 min. Then, it was elevated at a rate of 80 °C min^{-1} to 240 °C, before being increased at 2 °C min^{-1} until 290 °C and finally, maintained for 2 min at 290 °C. The ion source and transfer line temperatures were set to 270 °C and 280 °C, respectively. Mass detector was operated in scan mode. Identification of the FAME in the sample extracts was achieved by mass spectrum and GC retention time comparison with reference standards. The activities of FA elongases and desaturases were estimated, assessing established product to precursor metabolic ratios for each reaction [32–34]. In addition, the lipogenic index was calculated as the ratio C16:0/C18:2n6c [35,36].

2.9. Statistical Analysis

Quantitative data were analyzed using GraphPad Prism 6 (GraphPad Software Inc., San Diego, CA, USA) and statistical analysis of the results was performed by an unpaired *t*-test. Data is expressed as mean \pm standard error of the mean (SEM) and considered significant at a *p*-level of 0.05 or less. The study was performed according to the criteria of the Investigation and Ethics Committee of the Hospital Clínic of Barcelona.

3. Results

3.1. Characterization of CeO₂NPs

A description of the characterization of the CeO₂NPs used in this study has been published previously [27]. Briefly, the measured Z-Potential of CeO₂NPs was +40 mV at the final synthesis pH (pH = 6). The X-ray diffraction pattern showed pure CeO₂NPs with the typical peak broadening characteristic of nanosized particles. In this synthesis, CeO₂NPs obtained are monodisperse with an average of 4 \pm 1 nm size, as determined by TEM. In these conditions, the high surface energy of the NPs makes their electrical double layer unable to keep them apart and small agglomerates are formed. To avoid that, their immediate albuminization as they are formed, once the extreme initial pH of the solution is reduced (from pH 12 to pH 6), is key. HSA conjugation on the surface of the CeO₂NPs has been characterized by the increase in DLS and modification of the Z-Potential (from +40 mV of NPs as synthesized to –14 mV, which is the average Z-Potential value of the HSA (Figure 1).

3.2. Cellular Uptake of CeO₂NPs

Transmission electron microscopy was used to evaluate the association between HepG2 cells and incubation with CeO₂NPs (10 μ g/mL) for 24 h. TEM images revealed the presence of CeO₂NPs inside the cells, mainly in membrane-bound compartments and to a lesser extent, free in the cytoplasm (Figure 2). The presence of CeO₂NPs is revealed in the dark-field images since the high contrast of cerium oxide (CeO₂) crystals allowed them to be easily distinguished (as bright spots) from other cellular structures. The confinement of CeO₂NPs mainly in vacuoles or endosome-like organelles

suggested their presence in secretory compartments. These structures were not observed in the TEM images obtained from controls cells incubated without CeO₂NPs.

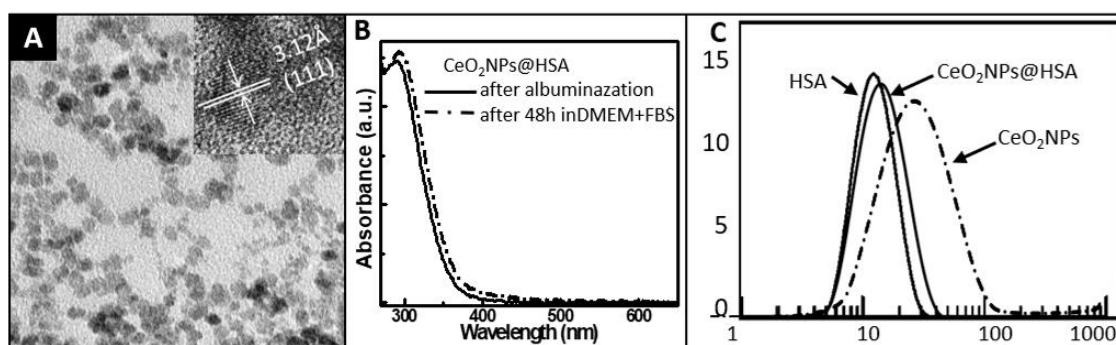


Figure 1. CeO₂NPs characterization. (a) Transmission electron microscopy (TEM) and high-resolution transmission electron microscopy (HR-TEM) (inset) showing the as-synthesized cerium oxide (CeO₂) nanocrystals of 4±1 nm; (b) UV-VIS spectroscopy of CeO₂NPs after conjugation to Human Serum Albumin (HSA) (CeO₂NPs@HSA) and the same nanoparticles (NPs) after 48 h in model physiological media (DMEM + Fetal Bovine Serum at 10% v/v). The similar spectra through time shows the stability in the physiological media of the NPs used; (c) Dynamic light scattering (DLS) of CeO₂NPs as synthesized, HSA, and CeO₂NPs@HSA. While the spectrum of CeO₂NPs shows a large presence of agglomerated NPs, the similar spectra of HSA and CeO₂NPs@HSA rules out the presence of CeO₂ aggregates. Note, that all samples have been purified before measurement.

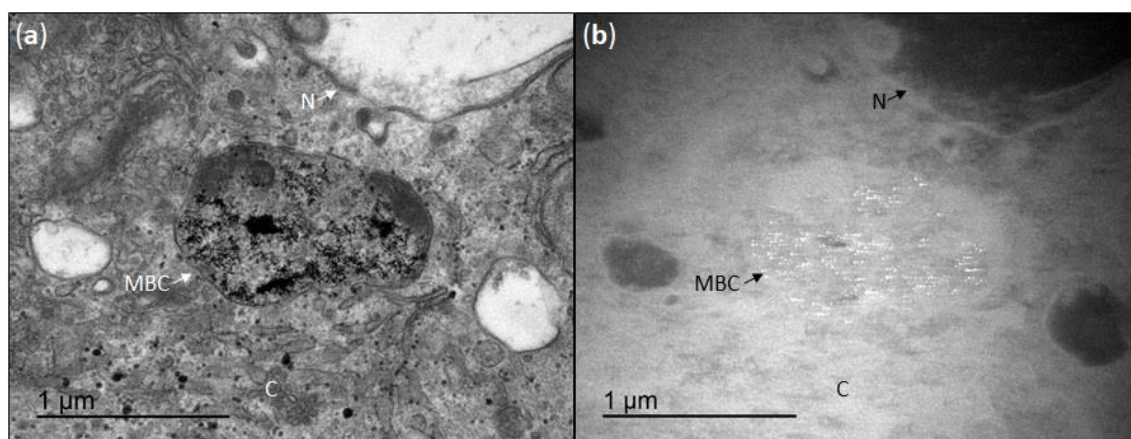


Figure 2. Cellular uptake of CeO₂NPs. (a) Transmission electron microscopy image of CeO₂NPs in HepG2 cells that were incubated for 24 h at a CeO₂NPs concentration of 10 μg/mL; (b) the same image obtained under dark-field exposure, since the high contrast of the CeO₂NPs allows them to be easily distinguished. MBC indicates a membrane-bound compartment, N the nucleus and C the cytoplasm.

3.3. Effect of CeO₂NPs in the Viability of HepG2 Incubated with H₂O₂

To evaluate cellular CeO₂NPs protection from H₂O₂-induced cytotoxicity in human hepatic cells, HepG2 cells were incubated with H₂O₂ and cellular viability was analyzed in the presence of CeO₂NPs or vehicle. Oxidative stress induced with a 1.5 mM H₂O₂ produced a reduction in cell viability of 14% (control 100% ± 1.8% and H₂O₂ 85.8% ± 1.1% viability (mean ± SEM); *p* < 0.0001). In these conditions, CeO₂NPs treatment improved cell viability, from 85.8% ± 1.1% in the H₂O₂ condition to 99.6% ± 1.8% in cells exposed to H₂O₂ and treated with NPs (*p* < 0.0001), indicating that CeO₂NPs protect from the oxidative-stress-associated cell death induced by H₂O₂ in HepG2 cells (Figure S1A).

3.4. Effect of CeO₂NPs in the ROS Production of HepG2 Incubated with H₂O₂

HepG2 cells incubated with H₂O₂ (1.5 mM) increased ROS production by 25% (control 100% ± 3.9% and H₂O₂ 125.4% ± 3.3% (mean ± SEM); $p < 0.0001$), as determined by fluorescence spectrophotometry using the oxidant-sensitive dye 2',7'-DCF-DA. ROS production was significantly inhibited in the presence of CeO₂NPs (H₂O₂ 125.4% ± 3.3% and H₂O₂ with CeO₂NPs 109.8% ± 3.8% (mean ± SEM); $p = 0.006$). These results indicate that CeO₂NPs protect from the oxidative stress induced by H₂O₂ in HepG2 cells (Figure S1B).

3.5. Effect of CeO₂NPs in Cholesterol and Oxysterols Content of HepG2 Cells Treated with H₂O₂

Effects of CeO₂NPs in the cellular content of cholesterol and cholesterol oxidation products were evaluated in HepG2 cells treated with vehicle, HepG2 cells treated with H₂O₂ (1.5 mM) and HepG2 cells treated with H₂O₂ and CeO₂NPs (1.5 mM, 10 µg/mL). Figure 3A shows a chromatogram of cholesterol and cholesterol oxidation products obtained by GC-MS in HepG2 cells. Cholesterol content was approximately 1000-fold higher than cholesterol oxidation products. The most abundant oxysterol measured was 7-ketocholesterol, followed by 7β-hydroxycholesterol and 25-hydroxycholesterol. No significant differences in cholesterol content were observed between cells treated with vehicle, H₂O₂ or H₂O₂ and CeO₂NPs. In contrast, cells treated with H₂O₂ presented a higher content of 7β-hydroxycholesterol. Treatment with CeO₂NPs reduced the concentration of oxysterols, although this decrease was not statistically significant (Figure 3B). Similar results were obtained when the ratio of oxysterol/cholesterol was calculated.

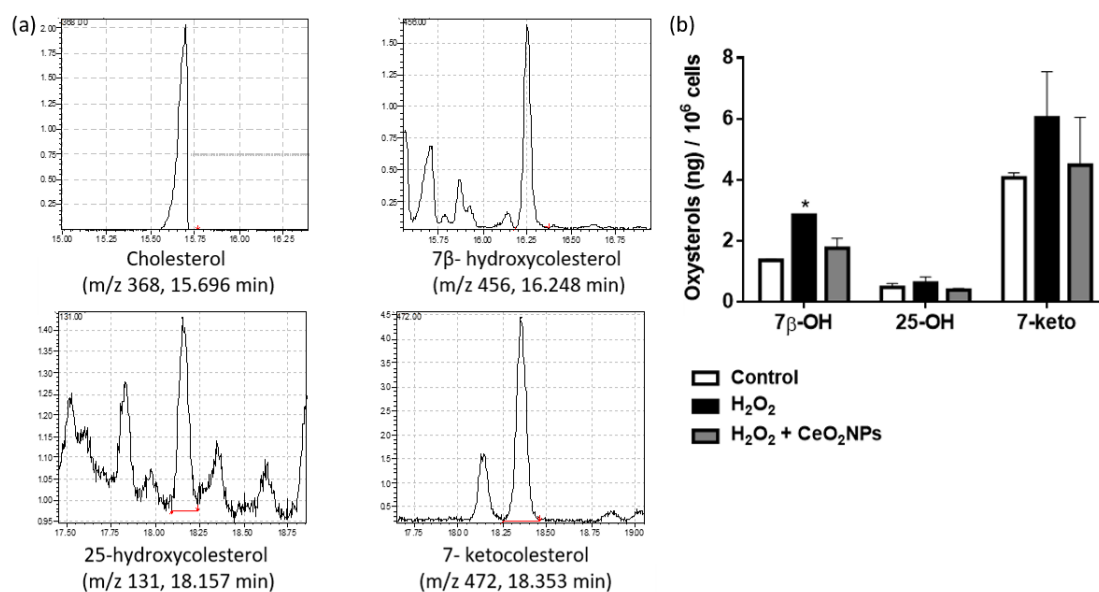


Figure 3. (a) Gas chromatography mass spectrometry chromatograms of cholesterol and its oxidation products in HepG2 cells; (b) oxysterols content in HepG2 cells treated with vehicle, H₂O₂ (1.5 mM) and H₂O₂ and CeO₂NPs (1.5 mM; 10 µg/mL). * $p < 0.05$ compared with control.

3.6. Effects of CeO₂NPs in Total FA Content of HepG2 Cells Treated with Oleic and Palmitic Acid

Oleic and palmitic acid treatment of HepG2 was used as an in vitro model to investigate the effect of CeO₂NPs in steatosis. HepG2 cells were exposed to 1.33 mM oleic acid (OA) and 0.67 mM palmitic acid (PA) for 24 h and intracellular accumulation of total FAs was measured by GC-MS. A chromatogram showing FAs in HepG2 cells is presented in Figure 4A. Consistent with the induction of the steatosis, total FAs content in HepG2 cells was increased in cells exposed to OA and PA in comparison to those exposed to vehicle (Figure 4B). Treatment with CeO₂NPs of cells exposed to OA

and PA produced a significant reduction of total saturated FAs (Figure 4C), while the total amount of unsaturated FAs was not significantly reduced (Figure 4D).

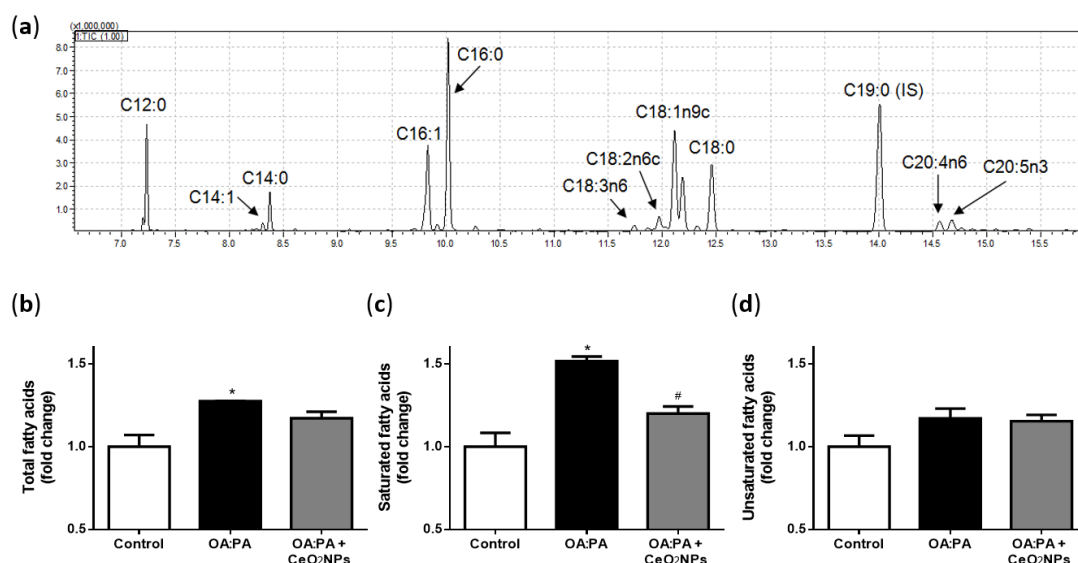


Figure 4. (a) Gas chromatography–mass spectrometry chromatogram of fatty acids in HepG2 cells. Content of total fatty acids (b), saturated fatty acids (c) and unsaturated fatty acids (d) in HepG2 cells exposed to vehicle (control), oleic acid:palmitic acid (OA:PA) (1.33:0.67 mM) and OA:PA with CeO₂NPs (10 µg/mL). * $p < 0.05$ compared with control; # $p < 0.05$ compared with OA:PA.

3.7. CeO₂NPs Induce Specific Changes in the FA Metabolism of Steatotic HepG2 Cells

Analysis of the individual FA species showed that, compared to normal cells, HepG2 cells exposed to OA and PA presented significant elevations in the intracellular content of different FA. As represented in Figure S2 and Table S1 (Supplementary Material), OA and PA incubation increased the cell content of C16:0, C18:0, C18:1n9c, C20:0, C20:1n9, C20:2n6, C20:5n3, C22:6n3 and C24:1n9. Interestingly, CeO₂NPs treatment of cells exposed to OA and PA decreased the cell content of most of these FA. Thus, CeO₂NPs treatment resulted in a 26% and 35% significant reduction of the highly abundant saturated FAs C16:0 and C18:0, respectively, and also, significantly decreased the content of very-long-chain saturated FA C23:0 by 58% (Figure 5). Regarding unsaturated FA, CeO₂NPs reduced the content of most FAs consisting of more than 18 carbon atoms, such as C20:1n9, C20:2n6, C20:3n6, C20:4n6, C20:5n3, C22:6n3 and C24:1n9 (Figure 6). In contrast, C18:3n3 and C18:3n6 content increased 44% and 10%, respectively, in cells treated with CeO₂NPs.

In order to determine the mechanism of CeO₂NPs antisteatotic effect, metabolic pathways of FAs were investigated. The activities of the main FA elongases (elongation of very-long-chain fatty acids 5 and 6 (ELOVL5 and ELOVL6)), and desaturases (steryl-CoA desaturase 1 (SCD1) and fatty acid desaturase 1 and 2 (FADS1 and FADS2)), were estimated by measuring the ratios between their products and substrates (Figure 7). Results showed that steatotic HepG2 cells presented an elevation of the lipogenic index C16:0/C18:2n6, which was associated with an activation of the elongase ELOVL5 and an inhibition of the desaturase SCD1 activities. CeO₂NPs treatment reduced the lipogenic index and reversed the changes in the elongase and desaturase activities induced by OA and PA. In addition, steatosis-induced elongation and desaturation towards the n-3 and n-6 pathway were normalized after steatotic cells were treated with CeO₂NPs. Scheme 1 shows specific changes in FA metabolism induced by CeO₂NPs in steatotic cells.

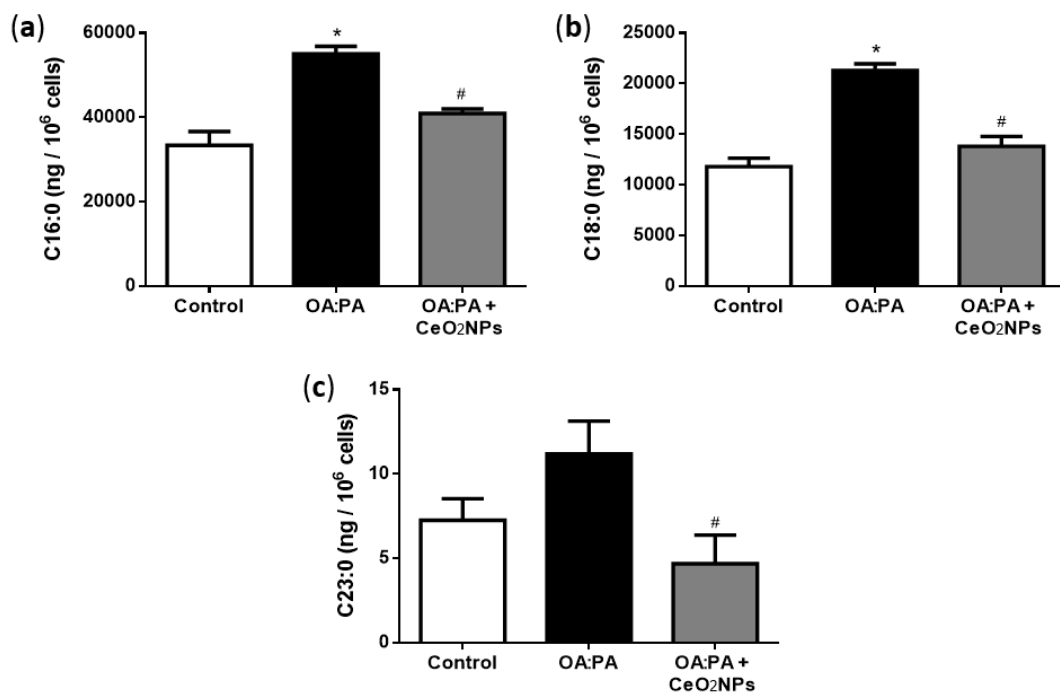


Figure 5. Palmitic (C16:0) (a), stearic (C18:0) (b) and tricosanoic (C23:0) (c) acid content in control cells, cells incubated with OA:PA (1.33:0.67 mM) and cells incubated with OA:PA treated with CeO₂NPs (10 µg/mL). * $p < 0.05$ compared with control; # $p \leq 0.05$ compared with OA:PA.

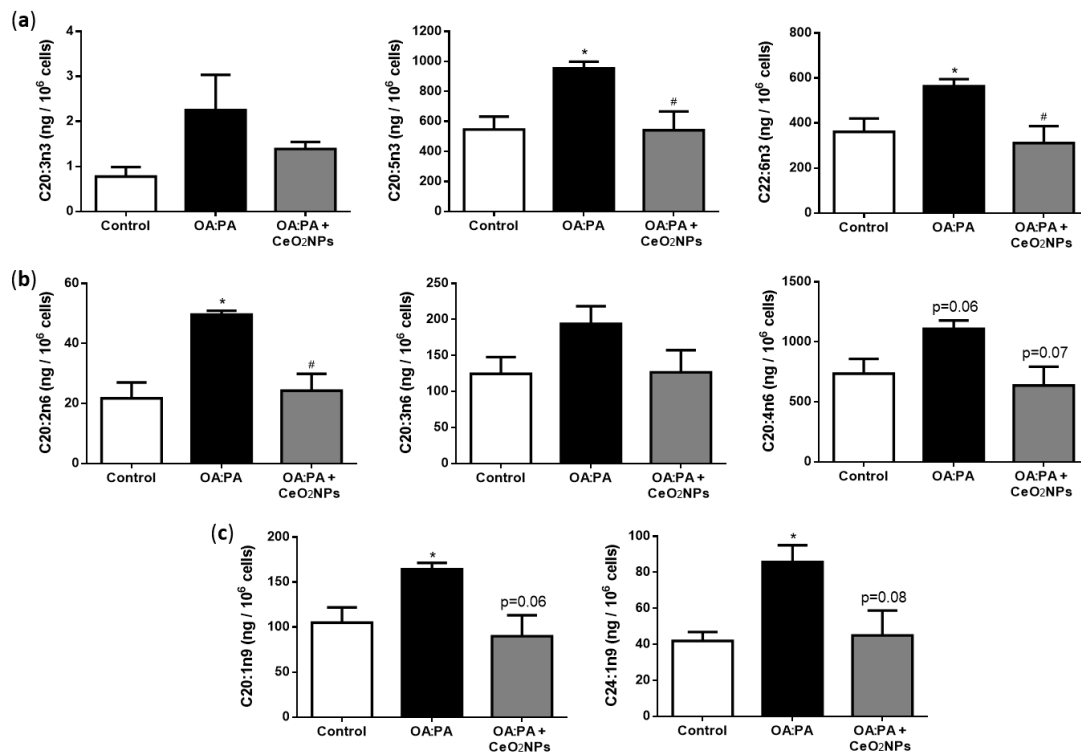


Figure 6. Cell content of n-3 (a), n-6 (b) and n-9 (c) unsaturated fatty acids larger than 18 carbons in control cells, cells incubated with OA:PA (1.33:0.67 mM) and cells incubated with OA:PA treated with CeO₂NPs (10 µg/mL). * $p < 0.05$ compared with control; # $p \leq 0.05$ compared with OA:PA.

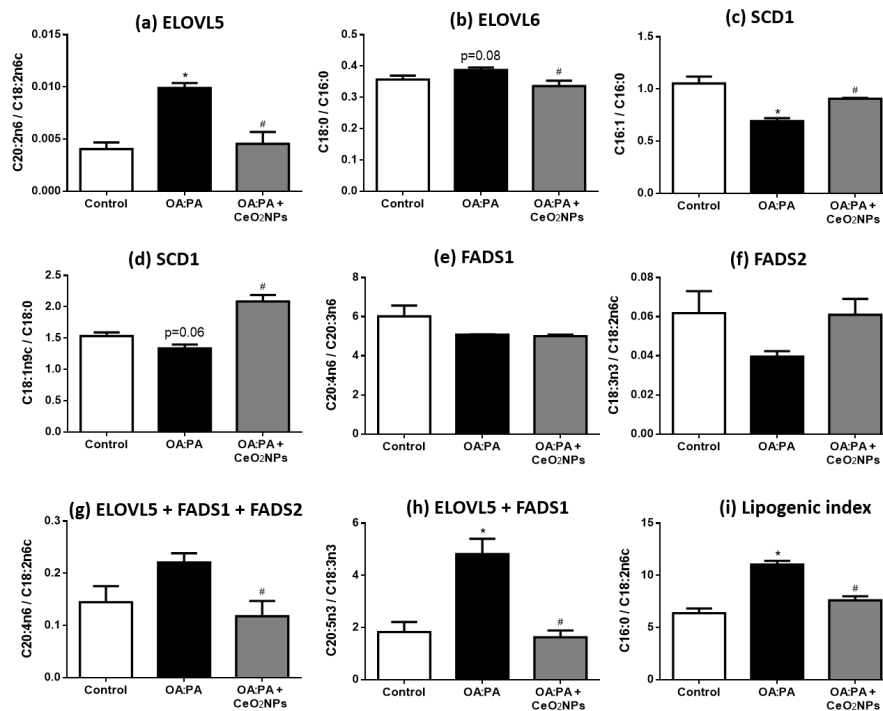
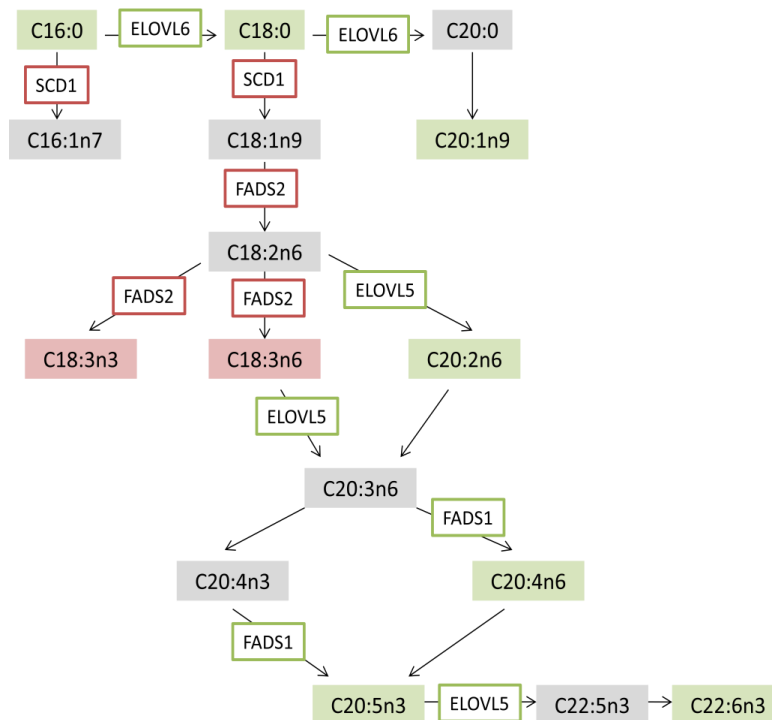


Figure 7. Fatty acid elongase and desaturase activities and lipogenic index in control cells, cells incubated with OA:PA (1.33:0.67 mM) and cells incubated with OA:PA treated with CeO₂NPs (10 µg/mL). C20:2n6/C18:2n6c (ELOVL5) (a); C18:0/C16:0 (ELOVL6) (b); C16:1/C16:0 (SCD1-C16:0) (c); C18:1n9c/C18:0 (SCD1-C18:0) (d); C20:4n6/C20:3n6 (FADS1) (e); C18:3n3/C18:2n6c (FADS2) (f); C20:4n6/C18:2n6c (ELOVL5 + FADS1 + FADS2 n-6 pathway) (g); C20:5n3/C18:3n3 (ELOVL5 + FADS1 n-3 pathway) (h); C16:0/C18:2n6c (lipogenic index) (i). * *p* < 0.05 compared with control; # *p* < 0.05 compared with OA:PA.



Scheme 1. Changes in fatty acid metabolism induced by CeO₂NPs in steatotic hepatic cells (HepG2 cells). Fatty acids in red are those up (increased content) and in green those down (decreased content) after CeO₂NPs treatment in our analyses. An increase in elongase and desaturase activities is framed in red and a decrease, in green.

4. Discussion

The current study shows that CeO₂NPs present protective cellular effects and reduce FA content in cultured human hepatic cells (HepG2 cells) cultivated under characteristic conditions of NAFLD. Specifically, cells were cultured under oxidative stress (H₂O₂ induced) or steatosis (OA:PA induced) in order to evaluate if CeO₂NPs presented a direct effect in these specific conditions. First, we evaluated whether CeO₂NPs were uptaken by HepG2 cells since, after intravenous administration of CeO₂NPs (3–20 nm), they have been observed to be located within hepatocytes of healthy mice [37] and rats with advanced liver disease [27]. In agreement with these *in vivo* studies, TEM images obtained in the current study revealed the uptake by HepG2 cells of CeO₂NPs, which were confined in vacuoles or endosome-like organelles. Similar observations have been reported when studying the uptake of CeO₂NPs by human hepatic cells C3A, in which confocal microscopy revealed a main perinuclear location of nanoparticles that suggested their presence in late endocytic or secretory compartments [38]. Furthermore, internalization of CeO₂NPs has been detected in human hepatic cells WRL-68 by flow cytometry [39].

Increased hepatic oxidative stress is a main physiopathological characteristic of NAFLD [40,41]. Increased ROS generation triggers lipid peroxidation, release of inflammatory cytokines and cell death. Patients with NASH display both an increase in ROS and nitrogen species production and a lack of endogenous antioxidant defenses [40]. In this regard, we next evaluated whether CeO₂NPs could directly decrease cellular oxidative stress in hepatic cells cultured with hydrogen peroxide (H₂O₂). CeO₂NPs produced a reduction in H₂O₂-induced cellular oxidative stress, as indicated by the decreased fluorescence of the oxidant-sensitive dye 2',7'-DCF-DA. This reduction in oxidative stress in CeO₂NPs-treated cells was accompanied by an improvement in cellular viability measured by the MTS assay. These results indicate that CeO₂NPs directly protect human hepatic cells from oxidative stress and the associated cellular injury. In agreement with this observation, Azari et al. [42] recently found that pretreatment of HepG2 cells with CeO₂NPs prevented oxidative and cellular damage caused by acrylamide, a toxic chemical compound present in cooked foods.

Also related to enhanced ROS production in NAFLD is the increase of hepatic oxidized cholesterol metabolites, which have been related to the progression of NAFLD [6,7]. Free cholesterol is susceptible to enzymatic and non-enzymatic oxidation, leading to the formation of a number of cholesterol oxidation products, including 25-hydroxycholesterol (enzymatic reaction) and 7β-hydroxycholesterol and 7-ketocholesterol (non-enzymatic) [43]. Our findings indicate an increase in 7β-hydroxycholesterol, 7-ketocholesterol and 25-hydroxycholesterol when HepG2 cells were exposed to an oxidant stimulus such as H₂O₂, suggesting that this is a suitable *in vitro* model for the study of cholesterol oxidation. However, when cells were co-incubated with CeO₂NPs, no significant reduction of oxysterols levels was observed. Correction of oxysterols levels by cholesterol lead to a similar trend. Further studies are necessary to ascertain the effect of CeO₂NPs on oxysterol formation in liver cells.

NAFLD is usually characterized by the presence of hepatic liver steatosis [9,10]. There is evidence derived from animal *in vivo* studies that CeO₂NPs treatment may reduce liver steatosis in different models of liver disease. Thus, in previous studies, our group first observed a reduction in liver steatosis in a CCl₄-induced model of liver fibrosis [27], and the same effect was reproduced in a methionine- and choline-deficient diet model of steatohepatitis in rats [44]. Also, oral administration of CeO₂NPs to a NAFLD rat model associated with neonatal monosodium-glutamate-induced obesity has been reported to decrease body weight and liver steatosis [28]. However, it is unknown whether these antisteatotic effects are only related to a systemic and/or hemodynamic improvement, or if CeO₂NPs may also behave as antisteatotic agents *per se*. In addition, it is unknown whether similar antisteatotic effects of CeO₂NPs to those observed in rats may be found in the human liver. Interestingly, there is evidence that CeO₂NPs may interfere in the normal FA metabolism of human-derived hepatocytes (HepG2 cells) [45,46], which represent the cell type in the liver that mainly accumulates FAs in NAFLD.

Therefore, in order to evaluate the ability of CeO₂NPs to reduce FA content in human hepatic cells, we next used an *in vitro* model of hepatocellular steatosis based on the administration of OA

and PA (2:1 molar ratio) to HepG2 cells. Induction of steatosis in hepatic cells through incubation with a mixture of OA (C18:1n9) and PA (C16:0) is an *in vitro* steatotic model widely used that is useful to evaluate antisteatotic effects in hepatic cells since it mimics the liver steatosis of NAFLD in patients [30,31,47,48]. OA, a monounsaturated FA, and PA, a saturated FA, are the most abundant FAs present in liver triglycerides [49] and serum [50]. These FAs have individual cell effects: OA is more steatogenic, while PA has a greater pro-apoptotic effect [31]. Exposure of HepG2 cells to a 2 mM mixture of OA:PA with a ratio of 2:1 for 24 h provides the maximal lipid accumulation with minimal cytotoxicity [30,31]. Gómez-Lechón et al. [30] found similar lipid accumulation in this *in vitro* model of hepatocellular steatosis when compared to hepatocytes from a human steatotic liver.

Our data show that HepG2 cells incubated with OA and PA increased C16:0, C18:0, C18:1n9c, C20:0, C20:1n9, C20:2n6, C20:5n3, C22:6n3 and C24:1n9. This is in agreement with a general induction of FA content previously observed in this model [31] and in the liver of patients with NAFLD [32,51–53]. However, C18:3n3 and C18:3n6 levels were not increased. In agreement with this, other research groups found low hepatic levels of C18:3n3 and C18:3n6 in animal models of NAFLD induced by a high-fat diet and CCl₄ [54] and a methionine- and choline-deficient diet [55], respectively.

PA (C16:0) increases the synthesis of C18:0 by elongation (ELOVL6), whereas OA (C18:1n9c) leads to higher content of C20:1n9 and C24:1n9, according to the metabolic elongation pathway of n-9 fatty acids. OA also promotes the formation of n-3 and n-6 long chain FAs through FADS2. Steatotic HepG2 cells presented decreased contents of C18:3n3 and C18:3n6, which may be associated with reduced FADS2 activity. By contrast, C20:4n6, C20:5n3 and C22:6n3 were markedly increased, supporting an induction of elongation and desaturation towards the n-3 and n-6 pathways. Overall, the increase in the lipogenic index C16:0 / C18:2n6c on HepG2 cells exposed to OA and PA is also in agreement with the induction of the steatotic metabolic process. Other indexes, such as C18:0/C16:0 (ELOVL6), which is increased in this model, have been shown to relate to the degree of liver steatosis in patients with NAFLD [51].

The antisteatotic effect of CeO₂NPs was proven by reduction of the highly abundant saturated FA C16:0 and C18:0 levels, together with a reduced content of most unsaturated FAs consisting of more than 18 carbon atoms. A differential effect of CeO₂NPs on C16:0 and C18:1n9 may be explained by the fact that C16:0 is not readily esterified and, to avoid toxicity, is converted to unsaturated FAs (such as C16:1n7 and C18:1n9) through elongation by ELOVL6 and desaturation by SCD1. Our data show that CeO₂NPs decreased ELOVL6 and increased SCD1 activities, which may explain why C16:1n7 and C18:1n9 levels were not reduced after CeO₂NPs treatment. Results suggest that CeO₂NPs may induce a more effective transformation of C16:0 to these unsaturated FAs to avoid toxicity.

The other significant FAs for which contents were reduced by CeO₂NPs treatment were those unsaturated FAs that consisted of more than 18 carbon atoms. The effect of CeO₂NPs in the reduction of these FAs was remarkable since many of them were completely normalized. This effect may be related to the observed inhibition of elongation and desaturation towards the n-3 and n-6 pathway. Importantly, CeO₂NPs reduced the eicosanoid precursors C20:4n6, C20:5n3 and C22:6n3, which are involved in the induction of inflammation and cell membrane integrity. However, provided that FAs consisting of more than 18 carbon atoms are preferentially oxidized in peroxisomes rather than in mitochondria, further research is necessary to evaluate whether CeO₂NPs may also promote peroxisome FA oxidation. In addition, C18:3n6 and C18:3n3 FA, which were not increased in steatotic HepG2 cells, exhibited an increase in their levels when cells were treated with CeO₂NPs, suggesting a CeO₂NPs-mediated induction of FADS2 activity. Finally, reduction of the lipogenic index by CeO₂NPs supports an overall antisteatotic effect.

One limitation of this study relates to the lack of evaluation of other factors that may also play a role in the pathophysiology of NAFLD, together with oxidative stress and lipid dysregulations. A significant example are the nuclear receptors, such as peroxisome proliferator-activated receptors (PPARs), liver X receptors (LXR) and farnesoid X receptors (FXR). They have been involved in the natural history of NAFLD, demonstrating that PPARs have one of the main roles in hepatic steatogenesis, LXR in

hepatic inflammation and FXR in hepatic fibrogenesis [56]. Furthermore, TEM images showing the cell uptake of CeO₂NPs were only obtained in basal conditions and there could be some changes in the localization of CeO₂NPs under oxidative stress and/or steatotic conditions. Finally, the antisteatotic effect of CeO₂NPs was evaluated in an OA:PA mixture and differential effects on steatosis induced by either OA alone or PA alone were not evaluated.

5. Conclusions

CeO₂NPs directly protect human hepatic cells from cell injury in conditions of oxidative stress and reduce FA content in steatotic conditions by inducing specific metabolic changes, suggesting that these NPs have great potential in the treatment of NAFLD.

Supplementary Materials: The following are available online at <http://www.mdpi.com/2218-273X/9/9/425/s1>.

Author Contributions: Conceptualization, M.P.-R., E.C., V.P., W.J. and G.C.; methodology, M.P.-R., E.C., M.Z., N.M., M.P., V.P., W.J. and G.C.; writing—original draft preparation, M.P.-R., E.C. and G.C.; writing—review and editing, M.P.-R., E.C., N.M., M.Z., M.P., G.F.-V., M.M.-R., V.P., W.J., and G.C.

Funding: This research was funded by Ministerio de Economía y Competitividad, grant number PI15-00077 to G.C. and SAF2016-75358-R to M.M.-R., co-financed by FEDER, European Union, “A way of making Europe”; “Secretaria d’Universitats i Recerca del Departament d’Empresa i Coneixement de la Generalitat de Catalunya, convocatòria d’Indústria del Coneixement modalitat B”, grant number 2018_PROD_00187 to W.J, cofinanced by the European Union through the European Regional Development Fund (ERDF), “A way of making Europe”; CIBERehd is financed by the Instituto de Salud Carlos III.; Wuyi University Funding for Hight Talents Introduction, grant number 2018TP010 to E.C. and 2018TP011 to M.Z.; Foundation from Department of Education of Guangdong Province, grant number 2016KCXTD005 and 2017KSYS010, to E.C. and M.Z. The APC was funded by Wuyi University Funding for Hight Talents Introduction, grant number 2018TP010 to E.C.

Acknowledgments: We thank Scientific and Technology Centers of the University of Barcelona (CCiT-UB) for their contribution to ultrastructural examinations by electron microscopy.

Conflicts of Interest: The authors declare no conflict of interest. The funders had no role in the design of the study; in the collection, analyses, or interpretation of data; in the writing of the manuscript, or in the decision to publish the results.

References

1. Friedman, S.L.; Neuschwander-Tetri, B.A.; Rinella, M.; Sanyal, A.J. Mechanisms of NAFLD development and therapeutic strategies. *Nat. Med.* **2018**, *24*, 908–922. [[CrossRef](#)] [[PubMed](#)]
2. Buzzetti, E.; Pinzani, M.; Tsochatzis, E.A. The multiple-hit pathogenesis of non-alcoholic fatty liver disease (NAFLD). *Metabolism* **2016**, *65*, 1038–1048. [[CrossRef](#)] [[PubMed](#)]
3. Italian Association for the Study of the Liver (AISF). AISF position paper on nonalcoholic fatty liver disease (NAFLD): Updates and future directions. *Dig. Liver Dis.* **2017**, *49*, 471–483. [[CrossRef](#)] [[PubMed](#)]
4. Duvnjak, M.; Lerotić, I.; Baršić, I.; Tomašić, V.; Jukić, L.V.; Velagić, V. Pathogenesis and management issues for non-alcoholic fatty liver disease. *World J. Gastroenterol.* **2007**, *13*, 4539–4550. [[CrossRef](#)] [[PubMed](#)]
5. Moore, J.B. From sugar to liver fat and public health: Systems biology driven studies in understanding non-alcoholic fatty liver disease pathogenesis. *Proc. Nutr. Soc.* **2019**, *78*, 290–304. [[CrossRef](#)] [[PubMed](#)]
6. Bellanti, F.; Villani, R.; Facciorusso, A.; Vendemiale, G.; Serviddio, G. Lipid oxidation products in the pathogenesis of non-alcoholic steatohepatitis. *Free Radic. Biol. Med.* **2017**, *111*, 173–185. [[CrossRef](#)] [[PubMed](#)]
7. Bellanti, F.; Villani, R.; Tamborra, R.; Blonda, M.; Iannelli, G.; di Bello, G.; Facciorusso, A.; Poli, G.; Iuliano, L.; Avolio, C.; et al. Synergistic interaction of fatty acids and oxysterols impairs mitochondrial function and limits liver adaptation during nafld progression. *Redox Biol.* **2018**, *15*, 86–96. [[CrossRef](#)] [[PubMed](#)]
8. Singh, S.; Osna, A.N.; Kharbanda, K.K. Treatment options for alcoholic and non-alcoholic fatty liver disease: A review. *World J. Gastroenterol.* **2017**, *23*, 6549–6570. [[CrossRef](#)]
9. Chalasani, N.; Younossi, Z.; Lavine, J.E.; Charlton, M.; Cusi, K.; Rinella, M.; Harrison, S.A.; Brunt, E.M.; Sanyal, A.J. The diagnosis and management of nonalcoholic fatty liver disease: Practice guidance from the American Association for the Study of Liver Diseases. *Hepatology* **2018**, *67*, 328–357. [[CrossRef](#)]
10. European Association for the Study of the Liver (EASL); European Association for the Study of Diabetes (EASD); European Association for the Study of Obesity (EASO). EASL-EASD-EASO clinical practice guidelines for the management of non-alcoholic fatty liver disease. *J. Hepatol.* **2016**, *64*, 1388–1402. [[CrossRef](#)]

11. Schubert, D.; Dargusch, R.; Raitano, J.; Chan, S.W. Cerium and yttrium oxide nanoparticles are neuroprotective. *Biochem. Biophys. Res. Commun.* **2006**, *342*, 86–91. [[CrossRef](#)] [[PubMed](#)]
12. Karakoti, A.; Singh, S.; Dowding, J.M.; Seal, S.; Self, W.T. Redox-active radical scavenging nanomaterials. *Chem. Soc. Rev.* **2010**, *39*, 4422. [[CrossRef](#)] [[PubMed](#)]
13. Nelson, B.C.; Johnson, M.E.; Walker, M.L.; Riley, K.R.; Sims, C.M. Antioxidant Cerium Oxide Nanoparticles in Biology and Medicine. *Antioxidants* **2016**, *5*, 15. [[CrossRef](#)] [[PubMed](#)]
14. Xue, Y.; Zhai, Y.; Zhou, K.; Wang, L.; Tan, H.; Luan, Q.; Yao, X. The Vital Role of Buffer Anions in the Antioxidant Activity of CeO₂Nanoparticles. *Chem. A Eur. J.* **2012**, *18*, 11115–11122. [[CrossRef](#)] [[PubMed](#)]
15. Pagliari, F.; Mandoli, C.; Forte, G.; Magnani, E.; Pagliari, S.; Nardone, G.; Licoccia, S.; Minieri, M.; Di Nardo, P.; Traversa, E. Cerium Oxide Nanoparticles Protect Cardiac Progenitor Cells from Oxidative Stress. *ACS Nano* **2012**, *6*, 3767–3775. [[CrossRef](#)] [[PubMed](#)]
16. Ribera, J.; Rodríguez-Vita, J.; Cordoba, B.; Portolés, I.; Casals, G.; Casals, E.; Jiménez, W.; Puentes, V.; Morales-Ruiz, M. Functionalized cerium oxide nanoparticles mitigate the oxidative stress and pro-inflammatory activity associated to the portal vein endothelium of cirrhotic rats. *PLoS ONE* **2019**, *14*, e0218716. [[CrossRef](#)]
17. Xu, C.; Qu, X. Cerium oxide nanoparticle: A remarkably versatile rare earth nanomaterial for biological applications. *NPG Asia Mater.* **2014**, *6*, e90. [[CrossRef](#)]
18. Korsvik, C.; Patil, S.; Seal, S.; Self, W.T. Superoxide dismutase mimetic properties exhibited by vacancy engineered ceria nanoparticles. *Chem. Commun.* **2007**, *14*, 1056. [[CrossRef](#)]
19. Pirmohamed, T.; Dowding, J.M.; Singh, S.; Wasserman, B.; Heckert, E.; Karakoti, A.S.; King, J.E.S.; Seal, S.; Self, W.T. Nanoceria exhibit redox state-dependent catalase mimetic activity. *Chem. Commun.* **2010**, *46*, 2736–2738. [[CrossRef](#)]
20. Heckert, E.G.; Seal, S.; Self, W.T. Fenton-Like Reaction Catalyzed by the Rare Earth Inner Transition Metal Cerium. *Environ. Sci. Technol.* **2008**, *42*, 5014–5019. [[CrossRef](#)]
21. Das, S.; Dowding, J.M.; Klump, E.K.; McGinnis, J.F.; Self, W.; Seal, S. Cerium oxide nanoparticles: Applications and prospects in nanomedicine. *Nanomedicine (Lond.)* **2013**, *8*, 1483–1508. [[CrossRef](#)] [[PubMed](#)]
22. Niu, J.; Wang, K.; Kolattukudy, P.E. Cerium oxide nanoparticles inhibits oxidative stress and nuclear factor- κ B activation in H9c2 cardiomyocytes exposed to cigarette smoke extract. *J. Pharmacol. Exp. Ther.* **2011**, *338*, 53–61. [[CrossRef](#)] [[PubMed](#)]
23. Corsi, F.; Caputo, F.; Traversa, E.; Ghibelli, L. Not Only Redox: The Multifaceted Activity of Cerium Oxide Nanoparticles in Cancer Prevention and Therapy. *Front. Oncol.* **2018**, *8*, 309. [[CrossRef](#)] [[PubMed](#)]
24. Kargozar, S.; Baino, F.; Hoseini, S.J.; Hamzehlou, S.; Darroudi, M.; Verdi, J.; Hasanzadeh, L.; Kim, H.W.; Mozafari, M. Biomedical applications of nanoceria: New roles for an old player. *Nanomedicine (Lond.)* **2018**, *13*, 3051–3069. [[CrossRef](#)] [[PubMed](#)]
25. Charbgoon, F.; Bin Ahmad, M.; Darroudi, M. Cerium oxide nanoparticles: Green synthesis and biological applications. *Int. J. Nanomed.* **2017**, *12*, 1401–1413. [[CrossRef](#)] [[PubMed](#)]
26. Heckman, K.L.; DeCoteau, W.; Estévez, A.; Reed, K.J.; Costanzo, W.; Sanford, D.; Leiter, J.C.; Clauss, J.; Knapp, K.; Gómez, C.; et al. Custom Cerium Oxide Nanoparticles Protect against a Free Radical Mediated Autoimmune Degenerative Disease in the Brain. *ACS Nano* **2013**, *7*, 10582–10596. [[CrossRef](#)] [[PubMed](#)]
27. Oró, D.; Yudina, T.; Fernández-Varo, G.; Casals, E.; Reichenbach, V.; Casals, G.; De La Presa, B.G.; Sandalinas, S.; Carvajal, S.; Puentes, V.; et al. Cerium oxide nanoparticles reduce steatosis, portal hypertension and display anti-inflammatory properties in rats with liver fibrosis. *J. Hepatol.* **2016**, *64*, 691–698. [[CrossRef](#)] [[PubMed](#)]
28. Kobyliak, N.; Virchenko, O.; Falalyeyeva, T.; Kondro, M.; Beregova, T.; Bodnar, P.; Shcherbakov, O.; Bubnov, R.; Caprnda, M.; Delev, D.; et al. Cerium dioxide nanoparticles possess anti-inflammatory properties in the conditions of the obesity-associated NAFLD in rats. *Biomed. Pharmacother.* **2017**, *90*, 608–614. [[CrossRef](#)]
29. Casals, E.; Gusta, M.F.; Piella, J.; Casals, G.; Jiménez, W.; Puentes, V. Intrinsic and Extrinsic Properties Affecting Innate Immune Responses to Nanoparticles: The Case of Cerium Oxide. *Front. Immunol.* **2017**, *8*, 970. [[CrossRef](#)]
30. Gomez-Lechon, M.J.; Donato, M.T.; Martínez-Romero, A.; Jiménez, N.; Castell, J.V.; O'Connor, J.E. A human hepatocellular in vitro model to investigate steatosis. *Chem. Interact.* **2007**, *165*, 106–116. [[CrossRef](#)]
31. Ricchi, M.; Odoardi, M.R.; Carulli, L.; Anzivino, C.; Ballestri, S.; Pinetti, A.; Fantoni, L.I.; Marra, F.; Bertolotti, M.; Banni, S.; et al. Differential effect of oleic and palmitic acid on lipid accumulation and apoptosis in cultured hepatocytes. *J. Gastroenterol. Hepatol.* **2009**, *24*, 830–840. [[CrossRef](#)] [[PubMed](#)]

32. Chiappini, F.; Coilly, A.; Kadar, H.; Gual, P.; Tran, A.; Desterke, C.; Samuel, D.; Duclos-Vallée, J.C.; Touboul, D.; Bertrand-Michel, J.; et al. Metabolism dysregulation induces a specific lipid signature of nonalcoholic steatohepatitis in patients. *Sci. Rep.* **2017**, *7*, 46658. [[CrossRef](#)] [[PubMed](#)]
33. Palladini, G.; Di Pasqua, L.G.; Berardo, C.; Siciliano, V.; Richelmi, P.; Mannucci, B.; Croce, A.C.; Rizzo, V.; Perlini, S.; Vairetti, M.; et al. Fatty Acid Desaturase Involvement in Non-Alcoholic Fatty Liver Disease Rat Models: Oxidative Stress versus Metalloproteinases. *Nutrients* **2019**, *11*, 799. [[CrossRef](#)] [[PubMed](#)]
34. Puri, P.; Wiest, M.M.; Cheung, O.; Mirshahi, F.; Sargeant, C.; Min, H.K.; Contos, M.J.; Sterling, R.K.; Fuchs, M.; Zhou, H.; et al. The Plasma Lipidomic Signature of Nonalcoholic Steatohepatitis. *Hepatology* **2009**, *50*, 1827–1838. [[CrossRef](#)] [[PubMed](#)]
35. Hudgins, L.C.; Hellerstein, M.; Seidman, C.; Neese, R.; Diakun, J.; Hirsch, J. Human fatty acid synthesis is stimulated by a eucaloric low fat, high carbohydrate diet. *J. Clin. Investig.* **1996**, *97*, 2081–2091. [[CrossRef](#)] [[PubMed](#)]
36. Paglialunga, S.; Dehn, C.A. Clinical assessment of hepatic de novo lipogenesis in non-alcoholic fatty liver disease. *Lipids Health Dis.* **2016**, *15*, 686. [[CrossRef](#)] [[PubMed](#)]
37. Hirst, S.M.; Karakoti, A.S.; Tyler, R.D.; Sriranganathan, N.; Seal, S.; Reilly, C.M. Anti-inflammatory Properties of Cerium Oxide Nanoparticles. *Small* **2009**, *5*, 2848–2856. [[CrossRef](#)]
38. Gaiser, B.K.; Fernandes, T.F.; Jepson, M.A.; Lead, J.R.; Tyler, C.R.; Baalousha, M.; Biswas, A.; Britton, G.J.; Cole, P.A.; Johnston, B.D.; et al. Interspecies comparisons on the uptake and toxicity of silver and cerium dioxide nanoparticles. *Environ. Toxicol. Chem.* **2012**, *31*, 144–154. [[CrossRef](#)] [[PubMed](#)]
39. Singh, R.; Singh, S. Redox-dependent catalase mimetic cerium oxide-based nanozyme protect human hepatic cells from 3-AT induced acatalasemia. *Colloids Surf. B Biointerfaces* **2019**, *175*, 625–635. [[CrossRef](#)]
40. Salomone, F.; Godos, J.; Zelber-Sagi, S. Natural antioxidants for non-alcoholic fatty liver disease: Molecular targets and clinical perspectives. *Liver Int.* **2016**, *36*, 5–20. [[CrossRef](#)]
41. Rolo, A.P.; Teodoro, J.S.; Palmeira, C.M. Role of oxidative stress in the pathogenesis of nonalcoholic steatohepatitis. *Free Radic. Biol. Med.* **2012**, *52*, 59–69. [[CrossRef](#)] [[PubMed](#)]
42. Azari, A.; Shokrzadeh, M.; Zamani, E.; Amani, N.; Shaki, F. Cerium oxide nanoparticles protects against acrylamide induced toxicity in HepG2 cells through modulation of oxidative stress. *Drug. Chem. Toxicol.* **2019**, *42*, 54–59. [[CrossRef](#)] [[PubMed](#)]
43. Serviddio, G.; Bellanti, F.; Villani, R.; Tamborra, R.; Zerbinati, C.; Blonda, M.; Ciacciarelli, M.; Poli, G.; Vendemiale, G.; Iuliano, L. Effects of dietary fatty acids and cholesterol excess on liver injury: A lipidomic approach. *Redox Biol.* **2016**, *9*, 296–305. [[CrossRef](#)] [[PubMed](#)]
44. Corominas, M.P.; Carvajal, S.; Oró, D.; Casals, E.; Varo, G.F.; Casals, G.; Parra-Robert, M.; Ribera, J.; Morales-Ruiz, M.; Puntès, V.; et al. FRI-334-Cerium oxide nanoparticles present antilipogenic and antiinflammatory effects in rats with diet-induced non-alcoholic fatty liver disease. *J. Hepatol.* **2019**, *70*, e543. [[CrossRef](#)]
45. Kitchin, K.T.; Grulke, E.; Robinette, B.L.; Castellon, B.T. Metabolomic effects in HepG2 cells exposed to four TiO₂ and two CeO₂ nanomaterials. *Environ. Sci. Nano* **2014**, *1*, 466–477. [[CrossRef](#)]
46. Kitchin, K.T.; Stirdivant, S.; Robinette, B.L.; Castellon, B.T.; Liang, X. Metabolomic effects of CeO₂, SiO₂ and CuO metal oxide nanomaterials on HepG2 cells. *Part Fibre Toxicol.* **2017**, *14*, 50. [[CrossRef](#)] [[PubMed](#)]
47. Sun, H.; Yang, W.; Tian, Y.; Zeng, X.; Zhou, J.; Mok, M.T.S.; Tang, W.; Feng, Y.; Xu, L.; Chan, A.W.H.; et al. An inflammatory-CCRK circuitry drives mTORC1-dependent metabolic and immunosuppressive reprogramming in obesity-associated hepatocellular carcinoma. *Nat. Commun.* **2018**, *9*, 5214. [[CrossRef](#)] [[PubMed](#)]
48. Ansari, A.; Bose, S.; Patra, J.K.; Shin, N.R.; Lim, D.W.; Kim, K.W.; Wang, J.H.; Kim, Y.M.; Chin, Y.W.; Kim, H. A Controlled Fermented Samjunghwan Herbal Formula Ameliorates Non-alcoholic Hepatosteatosis in HepG2 Cells and OLETF Rats. *Front. Pharmacol.* **2018**, *9*, 596. [[CrossRef](#)]
49. Araya, J.; Rodrigo, R.; Videla, L.A.; Thielemann, L.; Orellana, M.; Pettinelli, P.; Poniachik, J. Increase in long-chain polyunsaturated fatty acid n-6/n-3 ratio in relation to hepatic steatosis in patients with non-alcoholic fatty liver disease. *Clin. Sci.* **2004**, *106*, 635–643. [[CrossRef](#)]
50. Baylin, A.; Kabagambe, E.K.; Siles, X.; Campos, H. Adipose tissue biomarkers of fatty acid intake. *Am. J. Clin. Nutr.* **2002**, *76*, 750–757. [[CrossRef](#)]

51. Yamada, K.; Mizukoshi, E.; Sunagozaka, H.; Arai, K.; Yamashita, T.; Takeshita, Y.; Misu, H.; Takamura, T.; Kitamura, S.; Zen, Y.; et al. Characteristics of hepatic fatty acid compositions in patients with nonalcoholic steatohepatitis. *Liver Int.* **2015**, *35*, 582–590. [[CrossRef](#)] [[PubMed](#)]
52. Puri, P.; Baillie, R.A.; Wiest, M.M.; Mirshahi, F.; Choudhury, J.; Cheung, O.; Sargeant, C.; Contos, M.J.; Sanyal, A.J. A lipidomic analysis of nonalcoholic fatty liver disease. *Hepatology* **2007**, *46*, 1081–1090. [[CrossRef](#)] [[PubMed](#)]
53. Kotronen, A.; Seppänen-Laakso, T.; Westerbacka, J.; Kiviluoto, T.; Arola, J.; Ruskeepää, A.L.; Orešič, M.; Yki-Järvinen, H. Hepatic steatoyl-CoA desaturase (SCD)-1 activity and diacylglycerol but not ceramide concentrations are increased in the nonalcoholic human fatty liver. *Diabetes* **2009**, *58*, 203–208. [[CrossRef](#)] [[PubMed](#)]
54. Wang, X.; Cao, Y.; Fu, Y.; Guo, G.; Zhang, X. Liver fatty acid composition in mice with or without nonalcoholic fatty liver disease. *Lipids Health Dis.* **2011**, *10*, 234. [[CrossRef](#)] [[PubMed](#)]
55. Ma, C.; Kesarwala, A.H.; Eggert, T.; Medina-Echeverz, J.; Kleiner, D.E.; Jin, P.; Stroncek, D.F.; Terabe, M.; Kapoor, V.; ElGindi, M.; et al. NAFLD causes selective CD4(+) T lymphocyte loss and promotes hepatocarcinogenesis. *Nature* **2016**, *531*, 253–257. [[CrossRef](#)] [[PubMed](#)]
56. Ballestri, S.; Nascimbeni, F.; Romagnoli, D.; Baldelli, E.; Lonardo, A. The Role of Nuclear Receptors in the Pathophysiology, Natural Course, and Drug Treatment of NAFLD in Humans. *Adv. Ther.* **2016**, *33*, 291–319. [[CrossRef](#)] [[PubMed](#)]



© 2019 by the authors. Licensee MDPI, Basel, Switzerland. This article is an open access article distributed under the terms and conditions of the Creative Commons Attribution (CC BY) license (<http://creativecommons.org/licenses/by/4.0/>).